PAPER

Theoretical prediction of some layered Pa$_2$O$_5$ phases: structure and properties†

Tao Liu, [ab] Shichang Li, [a] Tao Gao*[a] and Bingyun Ao*[c]

Density functional theory (DFT) was used to predict and study protactinium pentoxide (Pa$_2$O$_5$), which presents a fluorite and layered protactinium oxide-type structure. Although the layered structure has been observed with the isostructural transition Nb and Ta metal pentoxides experimentally, the detailed structure and properties of the layered Pa$_2$O$_5$ are not clear and understandable. Our theoretical prediction explored some possible stable structures of the Pa$_2$O$_5$ stoichiometry according to the existing M$_2$O$_5$ structures (where M is an actinide Np or transition Nb, Ta, and V metal) and replacing the M ions with protactinium ions. The structural, mechanical, thermodynamic and electronic properties including lattice parameters, bulk moduli, elastic constants, entropy and band gaps were predicted for all the simulated structures. Pa$_2$O$_5$ in the β-V$_2$O$_5$ structure was found to be a competitive structure in terms of stability, whereas Pa$_2$O$_5$ in the ζ-Nb$_2$O$_5$ structure was found to be the most stable overall. This is consistent with Sellers's experimental observations. In particular, Pa$_2$O$_5$ in the ζ-Nb$_2$O$_5$ structure is predicted to be charge-transfer insulators. Furthermore, we predict that ζ-Nb$_2$O$_5$-structured Pa$_2$O$_5$ is the most thermodynamically stable under ambient conditions and pressure.

1. Introduction

The structure and properties of actinide-based oxides have been extensively studied using many theoretical[1–5] and experimental approaches[6–17] due to their technological importance in the nuclear material cycle. However, protactinium pentoxide (Pa$_2$O$_5$) is an underexplored area of the protactinium–oxygen phase diagram, and its practical applications have received little attention owing to its instability relative to the fluorite and layered protactinium oxides.[18,19] One of its intriguing features is that it represents the composition of a transition point between the fluorite and layered protactinium oxides, with reports of it forming in both types of structures. Since reports about the structure and properties of Pa$_2$O$_5$ are extremely limited in the literature, most likely owing to its scarcity, high radioactivity and toxicity, theoretical prediction provides a way to predict and study the structure and properties of this material.

In the actinide elements, uranium (U) exhibits rich oxide phases, such as UO$_2$, U$_2$O$_3$, U$_2$O$_5$, and U$_3$O$_8$,[20–27] and its two prominent oxidation states are U^{4+} and U^{6+}. Plutonium (Pu) has stable Pu^{4+}, Pu^{5+}, and Pu^{6+} oxidation states in aqueous solutions. Neptunium (Np) has two stable oxides, NpO$_2$ and Np$_2$O$_5$, corresponding to stoichiometric Np^{4+} and Np^{5+}, respectively. Protactinium (Pa), like actinide Np and the transition niobium (Nb), tantalum (Ta), and vanadium (V) metals, has the predominant oxidation state of Pa^{5+}. In particular, protactinium pentoxide is isostructural with the transition metals Nb and Ta, sharing a closed shell pentavalent oxidation state.[28] In addition, a study on Pa is considered to be a unique opportunity for studying the potential periodic properties of the actinide elements and their compounds with respect to their physics and chemistry, including structure and bonding. Wilson recently reported about protactinium as a potential intersection between the d-transition metals (Nb and Ta) and the 5f actinide elements U, Np and Pu owing to the participation of 5f and 6d orbitals cross in energy.[28] Although U, Np and Pu oxide systems are known, a detailed structural study of the layered protactinium pentoxide (Pa$_2$O$_5$) has not been systematically reported to date.

To develop new nuclear materials and understand their basic physical and chemical properties, a systematic study about the structure and properties of protactinium oxides is critical from a theoretical perspective. Pa$_2$O$_5$ is used for the preparation of metal Pa and other oxides (PaO and PaO$_2$), high temperature dielectrics for ceramic capacitors, in nuclear industry, *etc.*[19,29] Sellers *et al.*[19] experimentally showed that protactinium pentoxide has a fluorite structure and an orthorhombic structure. The fluorite Pa$_2$O$_5$ was prepared by heating the hydrated oxide in air (500 °C). Also, density data for fluorite

*a*Institute of Atomic and Molecular Physics, Sichuan University, Chengdu, 610065, China. E-mail: gaotao@scu.edu.cn

*b*School of Electronic and Communication Engineering, Guiyang University, Guiyang, 550005, China

*c*Science and Technology on Surface Physics and Chemistry Laboratory, P. O. Box 9072-35, Jiangyou, 621908, China. E-mail: aobingyun@caep.cn

Pa_2O_5 is not available, which suggests that it is more likely to be a defective fluorite PaO_2.[19] The orthorhombic Pa_2O_5, which is isostructural with Nb_2O_5 and Ta_2O_5, was obtained in the course of an attempt to prepare a fluoride by action of CuF_5 on the oxide (500 °C). Sellers' diffraction experiment suggested that Pa_2O_5 is a layered phase. Our theoretical work explores some possible structures of Pa_2O_5 by replacing the metal ions with protactinium ions from existing metal pentoxide structures. To study the potential structure and properties of layered Pa_2O_5, we report the structural, elastic, thermodynamic and electronic properties of some possible layered Pa_2O_5 phases using the Perdew–Burke–Ernzerhof generalized gradient approximation+U implemented in density functional theory (DFT). Our aim is to develop reliable structural models to aid the identification of possible phases and give a quantitative description of their relative stability.

2. Methodology

Theoretical calculations were performed using the projector augmented wave (PAW) method, as implemented in the Vienna *Ab Initio* Simulation Package (VASP).[30,31] The generalized gradient approximation (GGA) functional in the Perdew–Burke–Ernzerhof (PBE)[32] parametrization was adopted for structural optimization. The crystal structures of all systems concerned were relaxed using a Γ-centered k-mesh determined by requiring the product of the number of k points and the length of the lattice vectors to be ~30 Å and a large kinetic energy cutoff of 550 eV for plane waves. The energy convergence criterion was 10^{-6} eV, and the force convergence criterion was 10^{-4} eV Å^{-1}. After relaxation, the electronic structures were calculated with a kinetic energy cutoff of 500 eV.

The Dudarev approach[33] to the Perdew–Burke–Ernzerhof generalized gradient approximation GGA (PBE)+U implementation[34–38] was employed to enforce localization of the Pa 5f electrons. The effective U_{eff} (U–J) parameter of 4.0 eV (ref. 39) was used. This value was tested for PaO_2 and all simulated Pa_2O_5 structures, where the actinide (U, Np, and Pu) oxides in the literature[6,16,17,27,40–43] predicted good calculated structural properties. Spin–orbit coupling was not included in any of the calculations described herein since it has been previously demonstrated on actinide dioxides[10,44] that its effects on the structural properties and relative stabilities are inconsequential. The cutoff energy of 550 eV was reached for the convergence of the energy and the Γ-centered Monkhorst–Pack k-meshes of ζ-Nb_2O_5 $4 \times 6 \times 6$; Nb_2O_5 $4 \times 6 \times 4$; R-Nb_2O_5 $6 \times 6 \times 4$; B-Ta_2O_5 $4 \times 6 \times 6$; Z-Ta_2O_5 $6 \times 6 \times 6$; β-Ta_2O_5 $6 \times 6 \times 6$; β-V_2O_5 $3 \times 6 \times 4$; α-V_2O_5 $2 \times 6 \times 2$; and Np_2O_5 $4 \times 6 \times 4$ were automatically generated. The enthalpies of formation as a function of pressure and thermodynamic properties are presented in Fig. S1–S5.†

3. Results and discussion

3.1 Structural properties

The different structures of the layered Pa_2O_5 composition were simulated. Nb_2O_5,[45–47] Ta_2O_5,[48,49] V_2O_5,[50,51] Np_2O_5 (ref. 52)

structured M_2O_5 (where M is an actinide or transition metal) structures were investigated by replacing the metal ion with protactinium. All the relaxed simulated structures retained the coordination environments of the original M_2O_5 structures. We report the experimental structures of ζ-Nb_2O_5 and Np_2O_5 in comparison to our calculated structure of Pa_2O_5 in the ζ-Nb_2O_5 and Np_2O_5 structures. For Pa_2O_5 in the Np_2O_5 structure, the calculated lattice parameters (Table 1) are in good agreement with the experimental results of Np_2O_5, most likely because of the similarity between the protactinium and neptunium atomic radii (0.78 and 0.75 Å, respectively). Although the large protactinium cation (0.78 Å) substitutes the transition metal ions V (0.54 Å), Nb (0.69 Å) and Ta (0.69 Å), PBE+U demonstrates that the cell volume for Pa_2O_5 in the ζ-Nb_2O_5 structure is excellent compared to the experimental value of the original ζ-Nb_2O_5. An important reason for this is the change from transition metal ions to protactinium ions in the coordinate environment of the substitute position. The original ζ-Nb_2O_5 structure has an alternating MO_6-rich perovskite structure, and the replaced Pa_2O_5 in ζ-Nb_2O_5 phase was transformed into alternating MO_9 distorted hexahedron and quadrangular pyramid layers. The structural and mechanical properties of all the simulated systems are shown in Tables 1 and 2 and their relaxed structures are presented in Fig. 1–5.

Pa_2O_5 in Nb_2O_5 structure. The ζ-,[45] R-[46] and Nb_2O_5 (ref. 47) polymorphs were simulated. The ζ-Nb_2O_5 and Pa_2O_5 in the ζ-Nb_2O_5 structure are shown in Fig. 1a and b, respectively. Although the ζ-Nb_2O_5 structure is a skutterudite-like structure, the optimized Pa_2O_5 in the ζ-Nb_2O_5 phase can be considered a diamond-like (for 4 protactinium ions) structure, which has alternating MO_9 distorted hexahedron and quadrangular pyramid layers. As shown in Fig. 2a and b, the Nb_2O_5 and R-Nb_2O_5 phases are anatase-like structures and have layers of edge-sharing MO_6 octahedra, respectively. For the R-Nb_2O_5 structure, the layers are continuous in the c direction, while they are separated by 2 layers of a skutterudite-like structure for the Nb_2O_5 structure. All the protactinium ions for the R- and Nb_2O_5 phases are Pa^{5+} in the distorted octahedral coordination (Table 2).

Pa_2O_5 in Ta_2O_5 structure. We simulated the Z-[48] and β-Ta_2O_5 (ref. 49) polymorphs (Fig. 3a and b, respectively). Although many polymorphs exist for this oxide, they are generally very similar to Nb_2O_5. In particular, the structure of B-Ta_2O_5 is very similar to ζ-Nb_2O_5. β-Ta_2O_5 is a typical two-layer orthogonal structure. Z-Ta_2O_5 does not resemble the anatase structure and is more comparable to a distorted brookite structure (Fig. 2b). For the β-Ta_2O_5 and ζ-Nb_2O_5 structures, all the protactinium ions are Pa^{5+} in the distorted octahedral coordination (Table 2). In contrast, all the protactinium ions for the β-Ta_2O_5 structure are in the octahedral coordination.

Pa_2O_5 in V_2O_5 structure. Two polymorphs, α-[50] and β-V_2O_5,[51] are presented in Fig. 4. The β-V_2O_5 structure is built of infinite chains made of quadruple units of edge-sharing PaO_6 octahedra along the b axis. The chains are linked by sharing corners of two octahedra along the c axis. The α-V_2O_5 structure has a layered structure with orthorhombic symmetry consisting of PaO_5 square pyramids sharing edges and corners.

Table 1 Predicted properties of some layered Pa_2O_5 phases[a]

Phase	Method	Lattice parameters (Å)			Lattice parameters (deg)			Vol. (Å³)	Space group	E_{gap} (eV)	B (GPa)	E_{form} (eV)
		a	b	c	α	β	γ					
Pa_2O_5	Expt[19]	13.84	4.02	4.18	90.0	90.0	90.0					
ζ-Nb_2O_5	Expt[47]	12.740	4.883	5.561	90.0	105.02	90.0	334.12	C2/c (15)			
	PBE+U	12.620	5.387	5.387	90.0	114.68	90.0	332.72	C2/c (15)	2.67	198.33	−27.92
Nb_2O_5	PBE+U	14.446	4.282	15.035	90.0	163.64	90.0	262.02	P1 (1)	3.05	170.67	−26.41
R-Nb_2O_5	PBE+U	4.235	4.283	14.445	90.0	90.29	90.0	262.00	C2/m (12)	3.49	170.61	−26.40
Z-Ta_2O_5	PBE+U	6.302	4.077	6.517	90.0	107.37	90.0	159.82	C2/m (12)	2.21	282.70	−26.16
β-Ta_2O_5	PBE+U	6.991	4.048	8.474	90.0	90.0	90.0	239.84	Pccm (49)	1.93	178.87	−24.13
β-V_2O_5	PBE+U	6.645	3.937	7.412	90.0	78.57	90.0	190.05	P2_1/m (11)	3.28	198.91	−27.89
α-V_2O_5	PBE+U	11.576	4.220	10.664	90.0	90.0	90.0	520.93	Cmcm (63)	3.05	120.63	−25.01
Np_2O_5	Expt[52]	8.17	6.58	9.31	90.0	116.01	90.0	449.81	P2/c (13)			
	PBE+U	8.150	6.887	9.404	90.0	115.69	90.0	470.35	P2/c (13)	3.29	166.76	−26.95

[a] The enthalpy of formation ($E_{form} = E(Pa_2O_5) - 2E(Pa) - 5E(O)$) was calculated with respect to the energy of the Pa metal (8.72 eV per Pa) and the O_2 molecule (−4.90 eV per O). The energy of an O atom was predicted to be −4.90 eV, as calculated from an O_2 molecule in a 25 Å box using the Γ point.

Pa_2O_5 in Np_2O_5 structure. The simulated Np_2O_5 structure consists of 8 protactinium environments,[52] 4 with pentagonal bipyramidal coordination and 4 with octahedral coordination (Fig. 5 and Table 2). All the protactinium ions are predicted to be Pa^{5+}.

3.2 Stability

To confirm the thermodynamic stabilities of the predicted structures, the enthalpy of formation (E_{form}) for the simulated Pa_2O_5 structures are listed in Table 1. The relative enthalpy of formation E_{form} was calculated for each stoichiometry with respect to all the simulated Pa_2O_5 structures and gas O_2, as follows:

$$E_{form} = E(Pa_2O_5) - 2E(Pa) - 5E(O) \quad (1)$$

For clarity, the energies against the volume per Pa_2O_5 unit are plotted in Fig. 6. There is a clear dependence of the formation energy on the volume, with a decrease in stability for volumes smaller or larger than the most stable phases (ζ-Nb_2O_5).

The distribution of protactinium charges and protactinium coordination influence the stability. The ζ-Nb_2O_5-structured Pa_2O_5 is the most stable overall, although this structure contains all the Pa in a distorted hexahedron and quadrangular pyramid coordination. β-V_2O_5 was found to be just slightly less stable than ζ-Nb_2O_5 (0.03 eV) in terms of formation energy. The stability of the other phases follows the order of Np_2O_5 > Nb_2O_5 > R-Nb_2O_5 > Z-Ta_2O_5 > α-V_2O_5 > β-Ta_2O_5. Since Pa^{5+} prefers higher coordination numbers compared to the 6-fold distorted octahedral coordination, all the structures featuring protactinium ions entirely in the 6-fold coordination are consequently less stable. The V_2O_5-structured oxides are the least stable with the β-polymorph less stable than the α-V_2O_5 structure due to the presence of Pa in mixed oxidation states (Pa^{4+} and Pa^{5+}) compared to α-V_2O_5, which is comprised of only Pa^{5+} ions.

The DFT work from Molinari et al.[25] predicted that the Np_2O_5-structured U_2O_5 is the most stable among those considered under ambient conditions. However, the observed δ-U_2O_5 structure is found to be the second most stable. In particular, Pa_2O_5 in the β-V_2O_5 structure, given that it contains only octahedrally coordinated Pa, is closely followed by β-V_2O_5. The higher coordination numbers are also very similar to U_2O_5 since U is closely followed by R-Nb_2O_5.

These energetics show that Pa_2O_5 can crystallize in the ζ-Nb_2O_5 structure, but due to the relative instability of the Pa_2O_5 stoichiometry compared to the other protactinium oxides, it has not been synthesized or reported experimentally. The difficulty

Table 2 Coordination and charges of protactinium in the simulated Pa_2O_5 structures

Pa environment	No. of Pa environments per simulated unit cell							
	ζ-Nb_2O_5	Nb_2O_5	R-Nb_2O_5	Z-Ta_2O_5	β-Ta_2O_5	β-V_2O_5	α-V_2O_5	Np_2O_5
Pa^{5+} distorted octahedron		4	4				8	
Pa^{5+} octahedron					2			4
Pa^{5+} pentagonal bipyramid					2			4
Pa^{5+} distorted hexahedron and quadrangular pyramid	8			4				
Pa^{5+} 7-fold						2		
Pa^{4+} 7-fold						2		

Fig. 1 (a) Original ζ-Nb$_2$O$_5$ structure and (b) Pa$_2$O$_5$ in the ζ-Nb$_2$O$_5$ structures.

in synthesizing layered Pa$_2$O$_5$ is likely to stem from the fact that Pa^{5+} is more stable in the pentagonal bipyramidal coordination. One can also consider the formation of the studied Pa$_2$O$_5$ phases as a function of pressure, representing a range of conditions from low pressure to high pressure. The formation enthalpies as a function of pressure are presented in Fig. S1† and are normalized with respect to the most stable Pa$_2$O$_5$ (*i.e.*, the ζ-Nb$_2$O$_5$ structure) such that

$$\delta H_f = \Delta H(x) - \Delta H(\zeta\text{-Nb}_2\text{O}_5) \tag{2}$$

where x is the phase in question and $\Delta H(x)$ corresponds to E_{form} in Table 1. Interestingly, we predicted that at high pressure (above 100 kbar), Pa$_2$O$_5$ will be more thermodynamically stable in the ζ-Nb$_2$O$_5$ structure.

Using the density functional perturbation theory (DFPT)[53,54] calculated for each unit cell, the Helmholtz free energy, F_{vib} (Fig. S2†), vibrational entropy, S_{vib} (Fig. S3†), vibrational energy, E_{vib} (Fig. S4†), Helmholtz free energy, $F_{tot} = E_{form} + F_{vib}$ (Fig. S5†), and the heat capacity, C_v (Table 3), were evaluated. The Helmholtz free energy, F, entropy, S, internal energy, E, and
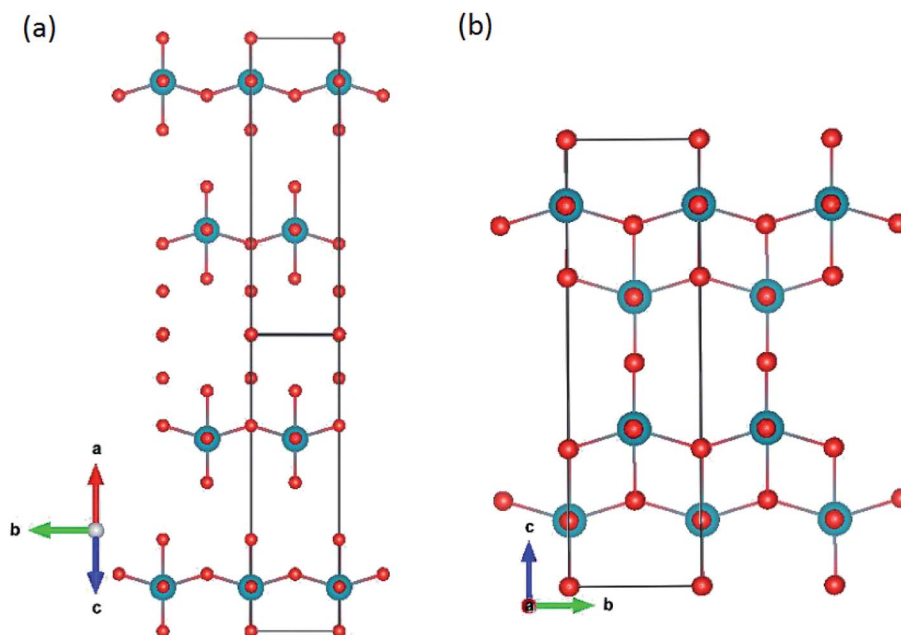

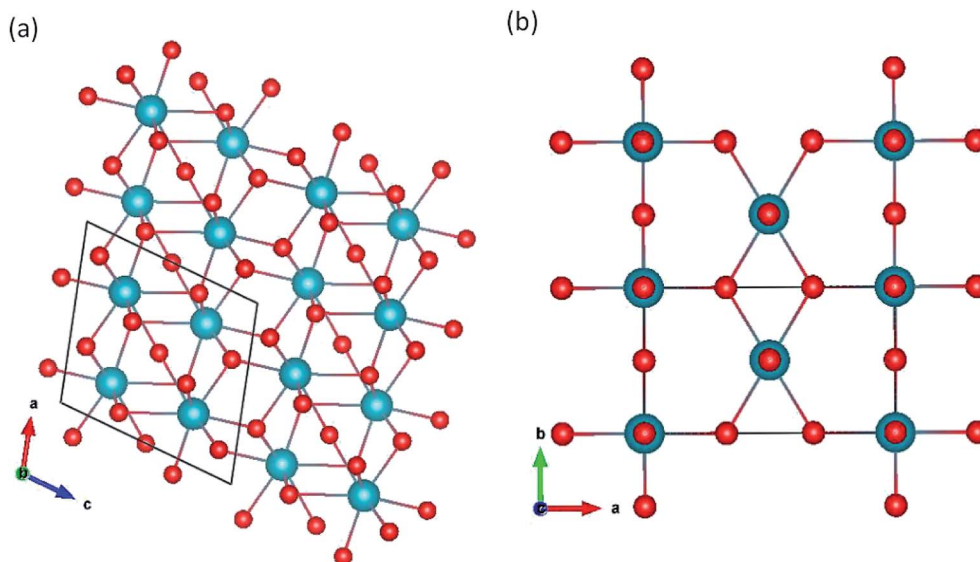Fig. 2 Pa$_2$O$_5$ in (a) Nb$_2$O$_5$ and (b) R-Nb$_2$O$_5$ structures.

Fig. 3 Pa_2O_5 in (a) Z-Ta_2O_5 and (b) β-Ta_2O_5 structures.

constant volume specific heat capacity, C_v, can be directly calculated as a function of temperature using the following equations:

$$F = rNk_BT \int_0^\infty g(\omega) \ln\left(2\sinh\left(\frac{\hbar\omega}{2k_BT}\right)\right) d\omega \quad (3)$$

$$S = rNk_BT \int_0^\infty g(\omega)\left[\frac{\hbar\omega}{2k_BT}\left(\coth\frac{\hbar\omega}{2k_BT}-1\right)\right.$$

$$\left.-\ln\left(1-\exp\left(-\frac{\hbar\omega}{k_BT}\right)\right)\right] d\omega \quad (4)$$

$$E = \frac{1}{2}Nr \int_0^\infty g(\omega)\hbar\omega \coth\frac{\hbar\omega}{2k_BT} d\omega \quad (5)$$

$$C_v = rNk_B \int_0^\infty g(\omega)\left(\frac{\hbar\omega}{2k_BT}\right)^2 \frac{\exp\left(\frac{\hbar\omega}{k_BT}\right)}{\left(\exp\left(\frac{\hbar\omega}{k_BT}\right)-1\right)^2} \quad (6)$$

where the indices ω is the phonon frequency, $g(\omega)$ is the normalized phonon density of states ($\int_0^\infty g(\omega)d\omega = 1$), r is the number of degrees of freedom in the primitive unit cell, and N is the number of primitive unit cells. $\hbar$ is Planck's constant, k_B is the Boltzmann constant, and T is the temperature in kelvin [K]. All these properties are expressed per Pa_2O_5 unit, and a sample of their values at 300 K is presented in Table 3. A full calculation of the phase stability for the Pa_2O_5 phases is beyond the scope of this work; however, our calculations show that the energy-minimized ζ-Nb_2O_5 phase has a lower enthalpy of formation (E_{form}) and vibrational entropy (S_{vib})

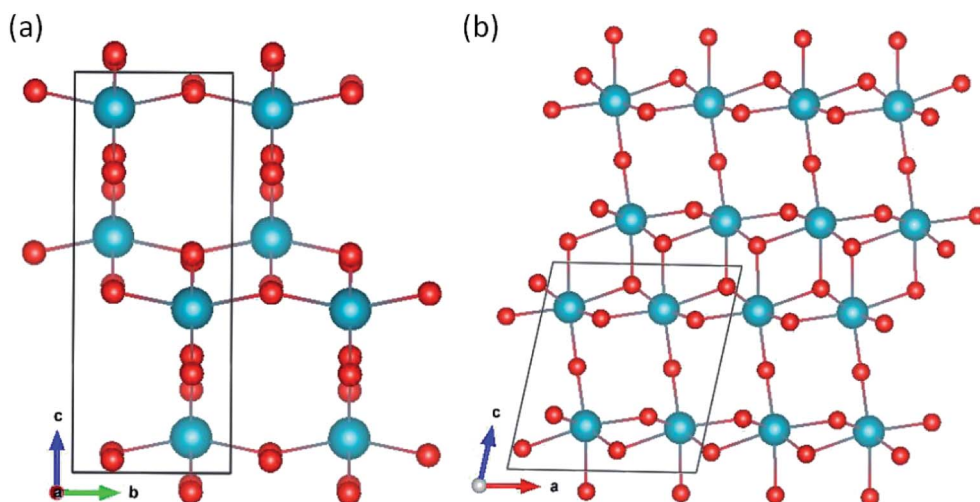**Fig. 4** Pa_2O_5 in (a) α-V_2O_5 and (b) β-V_2O_5 structures.
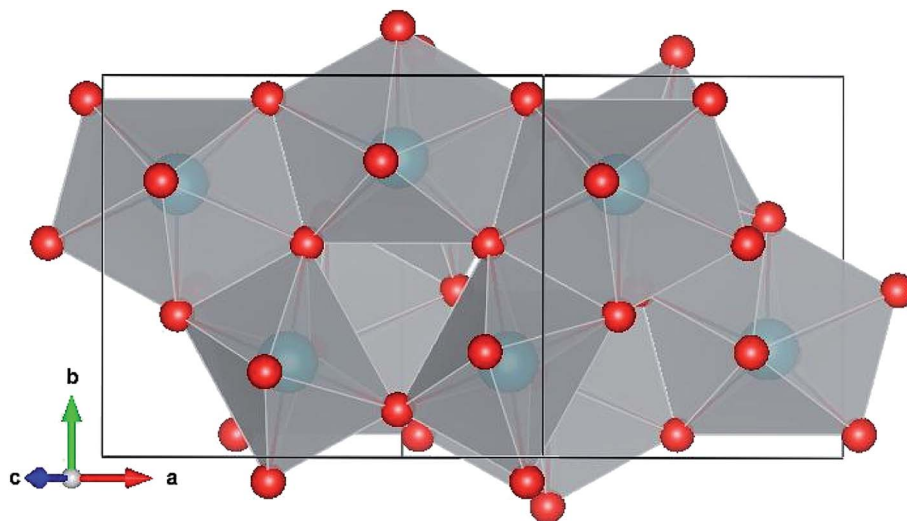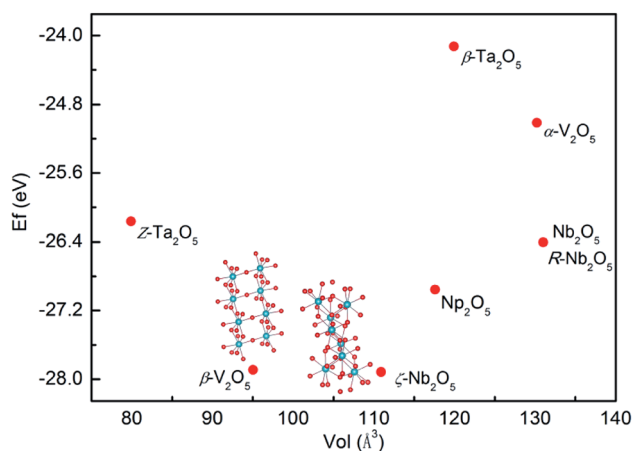
Fig. 5   Pa$_2$O$_5$ in the Np$_2$O$_5$ structure.

Fig. 6   Stability plot of the formation energy per Pa$_2$O$_5$ in electronvolt *vs.* volume per Pa$_2$O$_5$ unit. Phases are named with the original M$_2$O$_5$ structures for clarity.

than the other phases. Hence, using our calculated values, ζ-Nb$_2$O$_5$ is predicted to be the preferred structure at around 300 K and 0 bar (Fig. S5†).

Table 3   Predicted thermodynamic properties of some layered Pa$_2$O$_5$ phases at 300 K

Phase	F_{vib} (meV)	S_{vib} (meV K^{-1})	C_V (meV)	E_{vib} (meV)	F_{tot} (eV)
ζ-Nb$_2$O$_5$	214.2	1.43	135.5	612.0	−27.71
Nb$_2$O$_5$	18.9	2.03	145.3	628.7	−26.40
R-Nb$_2$O$_5$	45.3	1.95	145.4	629.3	−26.35
Z-Ta$_2$O$_5$	218.3	1.49	123.5	606.7	−25.94
β-Ta$_2$O$_5$	56.6	1.46	105.3	494.2	−24.07
β-V$_2$O$_5$	212.5	1.46	137.2	650.9	−27.68
α-V$_2$O$_5$	47.0	1.46	85.1	395.2	−24.96
Np$_2$O$_5$	107.6	1.72	140.7	622.8	−26.84

Fig. 7   Total and projected density of states of Pa$_2$O$_5$ in the ζ-Nb$_2$O$_5$ (a) and β-V$_2$O$_5$ (b) structures computed for the ground states in PBE+*U*. The Fermi energy stands at 0 eV.

3.3 Elastic properties

To evaluate the mechanical stability of all the simulated structures at ambient pressure, the calculated elastic constants are shown in Table S1,† which were calculated using the strain–stress relationship. The key criterion for the mechanical stability of a crystal is that the strain energy must be positive, which implies that the elastic constants should satisfy the generalized elastic stability criteria. In all the simulated structures, the *Pccm* phase (β-Ta$_2$O$_5$) is the only orthorhombic structure, and the others are monoclinic structures. For the orthorhombic structure, the nine independent elastic constants are C_{11}, C_{22}, C_{33}, C_{44}, C_{55}, C_{66}, C_{12}, C_{13} and C_{23}, and the corresponding mechanical stability criteria are given as[55]

$$C_{11} > 0, \ C_{11}C_{12} > C_{122}, \ C_{44} > 0, \ C_{55} > 0, \ C_{66} > 0, \ C_{11}C_{22}C_{33} + 2C_{12}C_{13}C_{23} - C_{11}C_{23}^2 - C_{22}C_{13}^2 - C_{33}C_{12}^2 > 0.$$

Meanwhile, the monoclinic structure has thirteen independent elastic constants (C_{11}, C_{22}, C_{33}, C_{44}, C_{55}, C_{66}, C_{12}, C_{13}, C_{23}, C_{15}, C_{25}, C_{35}, C_{46}) and the corresponding mechanical stability criteria are given as[55]

$$C_{11} > 0, \ C_{22} > 0, \ C_{33} > 0, \ C_{44} > 0, \ C_{55} > 0, \ C_{66} > 0, \ [C_{11} + C_{22} + C_{33} + 2(C_{12} + C_{13} + C_{23})] > 0, \ (C_{33}C_{55} - C_{35}^2) > 0, \ (C_{44}C_{66} - C_{46}^2) > 0, \ (C_{22} + C_{33} - 2C_{23}) > 0, \ [C_{22}(C_{33}C_{55} - C_{35}^2) + 2C_{23}C_{25}C_{35} - C_{23}^2C_{35} - C_{25}^2C_{33}] > 0, \ \{2[C_{15}C_{25}(C_{33}C_{12} - C_{13}C_{23}) + C_{15}C_{35}(C_{22}C_{13} - C_{22}C_{23}) + C_{25}C_{35}(C_{11}C_{23} - C_{12}C_{13})] - [C_{15}^2(C_{22}C_{33} - C_{23}^2) + C_{25}^2(C_{11}C_{33} - C_{13}^2) + C_{35}^2(C_{11}C_{22} - C_{12}^2)] + C_{55}(C_{11}C_{22}C_{33} - C_{11}C_{23}^2 - C_{22}C_{13}^2 - C_{33}C_{12}^2 + 2C_{12}C_{13}C_{23})\} > 0.$$

From the elastic constants listed in Table S1,† we find that the monoclinic phase of Pa$_2$O$_5$ in the ζ-Nb$_2$O$_5$ structures satisfies their respective mechanical stability criteria at ambient pressure, thus confirming their mechanical stability. However, the *Pccm* phase of Pa$_2$O$_5$ in the β-Ta$_2$O$_5$ structure is not the ground-state structure because this orthorhombic phase does not satisfy its mechanical stability criteria. Combining the thermodynamic and mechanical stability results, we conclude that the monoclinic phase is the ground-state structure for ζ-Nb$_2$O$_5$-structured Pa$_2$O$_5$ at ambient pressure. In addition, there is no evident correlation between the bulk moduli B and the volume (Vol.) or formation energy (E_{form}) of the layered Pa$_2$O$_5$ phases. Our work gives a high bulk modulus, B, for the ζ-Nb$_2$O$_5$-structured Pa$_2$O$_5$, but the bulk modulus of the Z-Ta$_2$O$_5$ structure is the largest.

3.4 Electronic properties

The experimental band gaps of the layered Pa$_2$O$_5$ phase are not currently available. In accordance with the higher layered oxide M$_2$O$_5$, all the structures are predicted to be ligand-to-metal charge-transfer (LMCT) insulators (O-2p to Pa-5f), with a conductance band composed of Pa 5f states and valence band comprised of O 2p states, with higher energy Pa 5f states at the core. To clearly describe the electronic properties of the most stable structure, the densities of states (DOS), projected density of states (PDOS) and band structure of Pa$_2$O$_5$ in the ζ-Nb$_2$O$_5$ and β-V$_2$O$_5$ structures are provided in Fig. 7 and S6.† These characteristics of Pa are attributed to its partially occupied 5f orbitals, which favors itinerancy for the early actinides. The appearance of significant Pa-5f/O-2p mixing arises from the increasing stabilization of the Pa 5f band due to incomplete shielding of the nuclear charge as one proceeds across the actinide series. There is a great variation in the predicted band gaps, with Pa$_2$O$_5$ in the ζ-Nb$_2$O$_5$ structure predicted to be 2.67 eV, which is more than the PaO$_2$ band gap of 1.40 eV.[56] As a comparison, the DOS and PDOS of Pa$_2$O$_5$ in the β-V$_2$O$_5$ structure are shown in Fig. 7b. Our PBE+U calculation predicts Pa$_2$O$_5$ in the β-V$_2$O$_5$ structure as a charge-transfer insulator with a band gap of 3.28 eV, which is bigger than the Pa$_2$O$_5$ in the ζ-Nb$_2$O$_5$ structure with a predicted gap of 0.61 eV. The presence of Pa 5f states in the valence band suggests a degree of covalent mixing with O 2p (fully ionic bonding would feature no overlapping states).

4. Conclusions

In this work, we presented some possible structures of the Pa$_2$O$_5$ stoichiometry starting from existing actinide and transition metal pentoxides based on density functional theory. Our calculations showed that the Pa$_2$O$_5$ structures prefer the Pa ions in homogeneous Pa^{5+} oxidation states and that all are in distorted hexahedron and quadrangular pyramid coordination. Our simulations predict that the ζ-Nb$_2$O$_5$-structured Pa$_2$O$_5$ is the most stable under zero temperature and ambient conditions. The observed β-V$_2$O$_5$ structure was found to be the second most stable structure. Thus, it is expected that protactinium can crystallize with the ζ-Nb$_2$O$_5$ structure; however, this has not been observed experimentally. ζ-Nb$_2$O$_5$-structured Pa$_2$O$_5$ is a charge-transfer insulator and its calculated band gap is 2.67 eV. Thus, this stoichiometry is clearly worthy of synthetic investigation since the ζ-Nb$_2$O$_5$ structure is found to be a stable phase. To better understand the fluorite to layered transformation, we will focus on using a more pragmatic approach to model fluorite-based Pa$_2$O$_5$ phases in future simulation work.

Conflicts of interest

There are no conflicts to declare.

Acknowledgements

References

1 T. Mark McCleskey, E. Bauer, Q. Jia, A. K. Burrell, B. L. Scott, S. D. Conradson, A. Mueller, L. Roy, X. Wen and G. E. Scuseria, *J. Appl. Phys.*, 2013, **113**, 013515.

2 T. Yaashita, N. Nitani, T. Tsuji and H. Inagaki, *J. Nucl. Mater.*, 1997, **245**, 72–78.

3 S. Kern, R. Robinson, H. Nakotte, G. Lander, B. Cort, P. Watson and F. Vigil, *Phys. Rev. B: Condens. Matter Mater. Phys.*, 1999, **59**, 104.

4 L. Asprey, F. Ellinger, S. Fried and W. Zachariasen, *J. Am. Chem. Soc.*, 1955, **77**, 1707–1708.

5 P. Santini, S. Carretta, G. Amoretti, R. Caciuffo, N. Magnani and G. H. Lander, *Rev. Mod. Phys.*, 2009, **81**, 807.

6 B. T. Wang, H. Shi, W. Li and P. Zhang, *Phys. Rev. B: Condens. Matter Mater. Phys.*, 2010, **81**, 045119.

7 Q. Yin and S. Y. Savrasov, *Phys. Rev. Lett.*, 2008, **100**, 225504.

8 P. Zhang, B. T. Wang and X. G. Zhao, *Phys. Rev. B: Condens. Matter Mater. Phys.*, 2010, **82**, 144110.

9 I. D. Prodan, G. E. Scuseria, J. A. Sordo, K. N. Kudin and R. L. Martin, *J. Chem. Phys.*, 2005, **123**, 014703.

10 X. D. Wen, R. L. Martin, T. M. Henderson and G. E. Scuseria, *Chem. Rev.*, 2012, **113**, 1063–1096.

11 X. D. Wen, R. L. Martin, L. E. Roy, G. E. Scuseria, S. P. Rudin, E. R. Batista, T. M. McCleskey, B. L. Scott, E. Bauer and J. J. Joyce, *J. Chem. Phys.*, 2012, **137**, 154707.

12 A. Bouasria, A. Zaoui, S. Ait Abderrahmane, S. Kacimi, A. Boukortt, M. Bejar and E. Dhahri, *Int. J. Comput. Mater. Sci. Eng.*, 2017, **6**, 1750006.

13 K. N. Kudin, G. E. Scuseria and R. L. Martin, *Phys. Rev. Lett.*, 2002, **89**, 266402.

14 I. D. Prodan, G. E. Scuseria and R. L. Martin, *Phys. Rev. B: Condens. Matter Mater. Phys.*, 2007, **76**, 033101.

15 D. Andersson, J. Lezama, B. Uberuaga, C. Deo and S. Conradson, *Phys. Rev. B: Condens. Matter Mater. Phys.*, 2009, **79**, 024110.

16 G. Jomard, B. Amadon, F. Bottin and M. Torrent, *Phys. Rev. B: Condens. Matter Mater. Phys.*, 2008, **78**, 075125.

17 B. Sun, P. Zhang and X. G. Zhao, *J. Chem. Phys.*, 2008, **128**, 084705.

18 K. T. Moore and G. van der Laan, *Rev. Mod. Phys.*, 2009, **81**, 235.

19 P. A. Sellers, S. Fried, R. E. Elson and W. Zachariasen, *J. Am. Chem. Soc.*, 1954, **76**, 5935–5938.

20 H. R. Hoekstra, S. Siegel and F. X. Gallagher, *J. Inorg. Nucl. Chem.*, 1970, **32**, 3237–3248.

21 N. A. Brincat, S. C. Parker, M. Molinari, G. C. Allen and M. T. Storr, *Dalton Trans.*, 2015, **44**, 2613–2622.

22 D. Andersson, G. Baldinozzi, L. Desgranges, D. Conradson and S. Conradson, *Inorg. Chem.*, 2013, **52**, 2769–2778.

23 C. Guéneau, M. Baichi, D. A. A. Labroche, C. Chatillon and B. Sundman, *J. Nucl. Mater.*, 2002, **304**, 161–175.

24 R. J. McEachern and P. Taylor, *J. Nucl. Mater.*, 1998, **254**, 87–121.

25 M. Molinari, N. A. Brincat, G. C. Allen and S. C. Parker, *Inorg. Chem.*, 2017, **56**, 4468–4473.

26 N. A. Brincat, S. C. Parker, M. Molinari, G. C. Allen and M. T. Storr, *Inorg. Chem.*, 2014, **53**(23), 12253–12264.

27 N. A. Brincat, M. Molinari, S. C. Parker, G. C. Allen and M. T. Storr, *J. Nucl. Mater.*, 2015, **456**, 329–333.

28 R. E. Wilson, S. Sio and V. Vallet, *Nat. Commun.*, 2018, **9**, 622.

29 L. R. Morss, N. M. Edelstein and J. Fuger, *The Chemistry of the Actinide and Transactinide Elements*, Springer, The Netherlands, 2010.

30 G. Kresse and J. Hafner, *Phys. Rev. B: Condens. Matter Mater. Phys.*, 1994, **49**, 14251.

31 G. Kresse and J. Furthmüller, *Phys. Rev. B: Condens. Matter Mater. Phys.*, 1996, **54**, 11169.

32 J. P. Perdew, K. Burke and M. Ernzerhof, *Phys. Rev. Lett.*, 1996, **77**, 3865.

33 S. Dudarev, G. Botton, S. Savrasov, C. Humphreys and A. Sutton, *Phys. Rev. B: Condens. Matter Mater. Phys.*, 1998, **57**, 1505.

34 V. I. Anisimov, J. Zaanen and O. K. Andersen, *Phys. Rev. B: Condens. Matter Mater. Phys.*, 1991, **44**, 943.

35 J. P. Perdew, A. Ruzsinszky, G. I. Csonka, O. A. Vydrov, G. E. Scuseria, L. A. Constantin, X. Zhou and K. Burke, *Phys. Rev. Lett.*, 2008, **100**, 136406.

36 V. I. Anisimov, F. Aryasetiawan and A. I. Lichtenstein, *J. Phys.: Condens. Matter*, 1997, **9**, 767.

37 A. Liechtenstein, *Phys. Rev. B: Condens. Matter Mater. Phys.*, 1995, **52**, R5467.

38 M. T. Czyżyk and G. A. Sawatzky, *Phys. Rev. B: Condens. Matter Mater. Phys.*, 1994, **49**, 14211.

39 T. Yamazaki and A. Kotani, *J. Phys. Soc. Jpn.*, 1991, **60**, 49–52.

40 V. I. Anisimov, A. I. Poteryaev, M. A. Korotin, A. O. Anokhin and G. Kotliar, *J. Phys.: Condens. Matter*, 1997, **9**, 7359.

41 Y. Yun, J. Rusz, M. T. Suzuki and P. Oppeneer, *Phys. Rev. B: Condens. Matter Mater. Phys.*, 2011, **83**, 075109.

42 K. O. Obodo and N. Chetty, *J. Phys.: Condens. Matter*, 2013, **25**, 145603.

43 X. D. Wen, R. L. Martin, G. E. Scuseria, S. P. Rudin, E. R. Batista and A. K. Burrell, *J. Phys.: Condens. Matter*, 2012, **25**, 025501.

44 J. Flitcroft, M. Molinari, N. Brincat, M. Storr and S. Parker, *Chem. Commun.*, 2015, **51**, 16209–16212.

45 T. S. Ercit, *Mineral. Petrol.*, 1991, **43**, 217–223.

46 B. O. Marinder, *Acta Chem. Scand.*, 1990, **44**, 123–134.

47 J. Spyridelis, P. Delavignette and S. Amelinckx, *Phys. Status Solidi B*, 1967, **19**, 683–704.

48 I. Zibrov, V. Filonenko, M. Sundberg and P. E. Werner, *Acta Crystallogr., Sect. B: Struct. Sci.*, 2000, **56**, 659–665.

49 L. Aleshina and S. Loginova, *Crystallogr. Rep.*, 2002, **47**, 415–419.

50 J. Cocciantelli, P. Gravereau, J. Doumerc, M. Pouchard and P. Hagenmuller, *J. Solid State Chem.*, 1991, **93**, 497–502.

51 V. Filonenko, M. Sundberg, P. E. Werner and I. Zibrov, *Acta Crystallogr., Sect. B: Struct. Sci.*, 2004, **60**, 375–381.

52 T. Z. Forbes, P. C. Burns, S. Skanthakumar and L. Soderholm, *J. Am. Chem. Soc.*, 2007, **129**, 2760–2761.

53 S. Baroni, S. De Gironcoli and A. D. Corso, *Rev. Mod. Phys.*, 2001, **73**, 515–562.

54 X. Gonze, *Phys. Rev. A: At., Mol., Opt. Phys.*, 1995, **52**, 1096–1114.

55 F. Mouhat and F. X. Coudert, *Phys. Rev. B: Condens. Matter Mater. Phys.*, 2014, **90**, 224104.

56 I. D. Prodan, G. E. Scuseria and R. L. Martin, *Phys. Rev. B: Condens. Matter Mater. Phys.*, 2007, **76**, 033101.